7-2020

Synthesis and Fabrication of Self-sustainable Triboelectric

Abu Masa Abdullah
The University of Texas Rio Grande Valley

Alejandro Flores
The University of Texas Rio Grande Valley

Aminur Rashid Chowdhury
The University of Texas Rio Grande Valley

Jianzhi Li
The University of Texas Rio Grande Valley

Yuanbing Mao
The University of Texas Rio Grande Valley

See next page for additional authors

Synthesis and Fabrication of Self-sustainable Triboelectric Energy Case for Powering Smart Electronic Devices

Credit Author Statement

Abu Musa Abdullah: Conceptualization, Methodology, Formal Analysis, Investigation, Resources, Writing-Original Draft, Visualization, Project Administration **Alejandro Flores:** Methodology, Investigation, Resources, Data Curation, Writing-Original Draft **Aminur Rashid Chowdhury:** Investigation, Visualization **Jianzhi Li:** Writing-Review and Editing **Yuanbing Mao:** Writing-Review and Editing **M. Jasim Uddin:** Validation, Supervision, Project Administration, Funding Acquisition

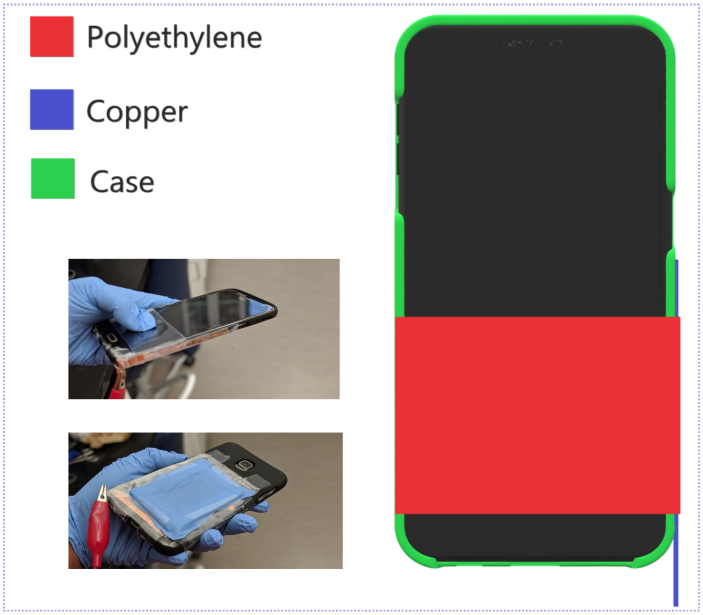
Polyethylene
Copper
Case

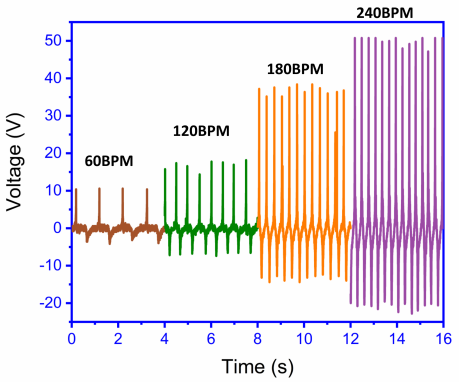
240BPM
180BPM
120BPM
60BPM
Voltage (V)
Time (s)
50
40
30
20
10
0
-10
-20
0
2
4
6
8
10
12
14
16

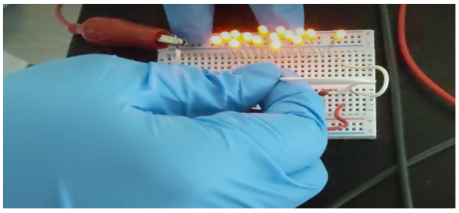

Synthesis and Fabrication of Self-sustainable Triboelectric Energy Case for Powering Smart Electronic Devices

Abu Musa Abdullah[1,2], Alejandro Flores[1,2], Aminur Rashid Chowdhury[1,3],Jianzhi Li[4], Yuanbing Mao[1,3], M. Jasim Uddin[1,3,*]

[1] Photonics and Energy Research Laboratory, The University of Texas Rio Grande Valley, 1201 W University Drive, Edinburg, Texas, TX-78539, USA

[2] Department of Mechanical Engineering, The University of Texas Rio Grande Valley, 1201 W University Drive, Edinburg, Texas, TX-78539, USA

[3] Department of Chemistry, The University of Texas Rio Grande Valley, 1201 W University Drive, Edinburg, Texas, TX-78539, USA

[4] Department of Manufacturing Engineering, The University of Texas Rio Grande Valley, 1201 W University Drive, Edinburg, Texas, TX-78539, USA

*Corresponding Author: M. Jasim Uddin (mohammed.uddin@utrgv.edu)

Abstract

In recent times, Triboelectric Nanogenerators (TENG) have attained the focus of the scientific community due to its potential as a medium to harvest mechanical energy from the ambient environment. Human motion has been attributed as a source of mechanical energy to drive electronic devices and sensors through TENG. Based on the principles of single electrode TENG, we have developed a Triboelectricity based Stepping and Tapping Energy Case (TESTEC) which magnifies the prospect to power touch electronic devices by utilizing finger tapping and stepping motion. This novel case was constructed with two single electrode TENG operating through the triboelectric mechanism between human skin and Polyethylene terephthalate(PET) film on the front part and Nitrile Butadiene Rubber(NBR) and PET film on the back part. This cost effective device was further tested by attaching with a cell phone at variable load frequency, airgap and finger combinations where the output response increased with the increased frequencies (60 to 240 BPM) and air gap (1cm to 5cm). Maximum output voltages of 14.8 V and 50.8 V were obtained for the front and back parts, respectively. Besides,

maximum output powers were observed to be 3.78 W/m^2 at 0.46 MΩ and 6.21 W/m^2 at 1.02 MΩ, respectively. Also, the device was tested by integrating with conventional electronic components including capacitors, bridge rectifiers and 15 LEDs. Based on the results, a electrical circuit has been proposed to power touch cell phones. The device was further modified using Silver (Ag) nanoparticles in the front part. The modified TESTEC provided higher output response compared to the primary TESTEC. The TESTEC can be a self sustainable way to power touch electronic devices which can reudce the necessity to charge electronics devices in the conventional way.

Keywords

Triboelectricity, Nanogenerator, Powering Smart Electronics, Self-sustainable Energy Case, Mechanical Energy Harvesting

Introduction

The advancement of information technology has significantly promoted electronic devices in everyday life [1,2]. Extensive usage of electronic device has been increasing day by day resulting greater demand of energy. This demand of energy will be doubled by the end of 2035 which is also expected to increase in an order of 1 GW per day till 2050 [3,4]. However, due to the limitation of natural resource and environmental pollution caused by energy production and consumption, experts are focusing towards sustainable development and green energy for meeting the energy demand for today and tomorrow [5–8]. One of the ways to meet up this demand can be harvesting unanimously available mechanical energy from the environment which is widely known as energy scavenging. Various effects like Piezoelectric, Electrostatic, Electromagnetic, Pyroelectric and triboelectric effects are generally being used for

harvesting this type of environment friendly energy [9–14]. Particularly, the recently invented Triboelectric Nanogenerators have been in great attention to the experts for powering electronic devices and sensory application through contact triboelectrification and electrostatic induction [15–17]. TENG was first developed by Fan *et al.* in 2012 after the introduction of the concept of nanogenerator in 2006 by Wang *et al.* [18,19]. Since then, TENG with low cost, high power density, light weight, good flexibility and good efficiency has been developed which in turn promoted its application in driving small electronics device and sensors [3,9,16,20–24]. The power density has been reported as high as 500 Wcm^{-2} by Zhu *et al.* while a ultra-high energy efficiency of 70.6% has been reported by Tang *et al.* [25,26].

Modern electronic devices like cellphones, tablets, calculators *etc*. are required to be small, lightweight and efficient in order to make them portable and competitive in the consumer market [27]. Electronic devices are getting lighter, thinner and better; but this has led to a sacrifice in the space-size of a device and due to this lack of space it is harder to improve this technology [28]. Contraction of space-size has reduced the space allotment for storage unit such as batteries which has led towards less capacity of the device to store energy. These problems can be solved by developing a self-sustaining and self-charging battery using energy from the ambient environment. Since, human motion can be affiliated to the usage of the electronic devices, utilizing the mechanical motion through TENG claims to be the solution of this problem [29–37].

In order to create a TENG that does not affect the ease of use, shape and efficiency of an electronic device, investigation has to be done for selecting the most proper materials that could address these requirements [10,38]. In this work, a cost-effective energy case of unique design including two single electrode TENG was constructed to utilize the energy from the mechanical

motion while using or carrying the touch electronic device and use this energy to power these smart devices. In the front part of the device a single electrode based TENG was fabricated for the front part of a cellphone without covering the screen and, at the same time, protecting it without affecting the functionality of the device, transparent materials were chosen as priority and as a second priority by their hardness and strength[39–43]. Selecting PET material as the best choice covering these requirements and looking for a new way to recycle it, it was found as the ideal material to create a TENG for the front part of the device [44]. This first TENG works with one fundamental principle proper of it, single-electrode mode [45–47]. By attaching PET on the screen of the cellphone and putting copper connected to a small surface of the material by one side of the cellphone is how this TENG is made. This TENG is activated by using human skin to touch the PET surface and harvesting the mechanical energy that is commonly applied to touch a screen of a cellphone and then transform it into electrical energy[48–50]. The front part was further modified using Ag nanoparticles over the PET film which was tested at 120 Beat Per Minute (BPM) load frequency. The output response was compared with the obtained results from the primary device as well.

The second nanogenerator is located on the back part. We wanted to take completely advantage of the mechanical energy created by a human so we developed a TENG that can take mechanical energy by walking[51,52]. This is made with NBR and Polyethylene. The polyethylene is placed on the back part of the smart phone, NBR, and a spacer that prevents each material from continually touching each other. NBR was used for fabricating the TENG at the back part as it gave good response with PET. It works through frictions as a single-electrode TENG [36]. The motion that is created by walking is enough to make these two materials touch each other. Combining the both parts, the device can be called Triboelectricity based Stepping

and Tapping Energy Case (TESTEC). TESTEC showed the potential to utilize the mechanical energy that is related to the daily life usage of smart electronic devices. The application of TESTEC into different electronics seeks to be the solution for the creation of cost effective and self-sustaining electronic devices for the near future[53].

Experimental Procedures

Synthesis of SETENG for Primary Testing

4cm X 3cm Cu films were used to synthesize SETENG for primary testing. Commercially available PET, PE and PP films of the same dimension were attached with the Cu films. An extension of the Cu film was added for attaching the device with alligator clips.

Polydimethylsiloxane (PDMS) based SETENG was synthesized using 2g PDMS (Sylgard 184 Silicone Elastomer Base) and 10wt% curing agent (Sylgard 184, Elastomer Curing Agent). The reagents were mixed using vortex mixer for proper mixing. Then the mixture was placed on the Cu film using Doctor's Blade technique following by drying in the room temperature for 36 hours.

Synthesis and device fabrication

The cellphone used for this experiment was a Samsung J5 and a case of the company Writeright for this phone as well. The materials used for the frontal part of the TESTEC were a commercial PET film and copper tape. The PET film was cut 8cm X 4cm leaving a small extra surface equality form to the side of it and then cleaned with ethanol. A copper tape was attached to one side of the device. Then the small extra surface previously left was bent and placed over the copper tape. The PET film was attached with tape from the exterior part.

The back part of the TESTEC was made with NBR (VWR), PET, and copper. A copper film was cut with 9cm x 6cm dimensions not bigger than the device. It was cleaned with ethanol and placed in the center on the back part properly attached with copper tape maintaining a connection with the copper tape previously attached to one of the sides of the device. A PET film was cut with the same dimensions of the copper foil, cleaned with ethanol and attached over the copper foil with tape. The material used for the spacer is Polyurethane foam, it was cut in a 5.5 cm x 7.5 cm with a thickness of 0.3 cm and then cut from the inside leaving a 0.8 cm of width giving us a shape of frame. After that it was attached with glue over the polyethylene film. The NBR film followed the same process cut with similar dimensions as the other materials, cleaned with ethanol and attached with copper tape.

The TESTEC was further modified using Ag nanoparticles on the PET film. Ag nanoparticles were sputtered on the PET film using a magnetron sputtering system (AJA International inc: ATC- Orion-5UHV) at rate of 0.5nm/sec (10nm thick). The modified PET film was then attached with the case like the previous steps discussed.

FTIR Characterization:

The Fourier Transform Infrared Spectra of the PET and NBR film were obtained using VERTEX 70v FTIR Spectrometer (Bruker) in Attenuated Total Reflection (ATR) mode. Transmittance of the both samples were recorded at wavelength from 450cm^{-1} to 4000cm^{-1}.

UV-Vis Characterization:

The UV-Vis spectra of the modified PET film were performed using Perkin Elmer Lambda 950 UV-Vis Spectrometer from 250cm^{-1} to 800cm^{-1}.

Measuring of Output:

The output voltage signal from the TESTEC was characterized with Tektronix TDS1001B digital oscilloscope, while the current signal was measured using low noise current pre amplifier (Stanford Research SR570). For further confirmation VersaSTAT 3 potentiostat and Tektronix A622 current probe were used for voltage and current measurement respectively. The entire test was carried out in ambient environment.

Results and Discuission

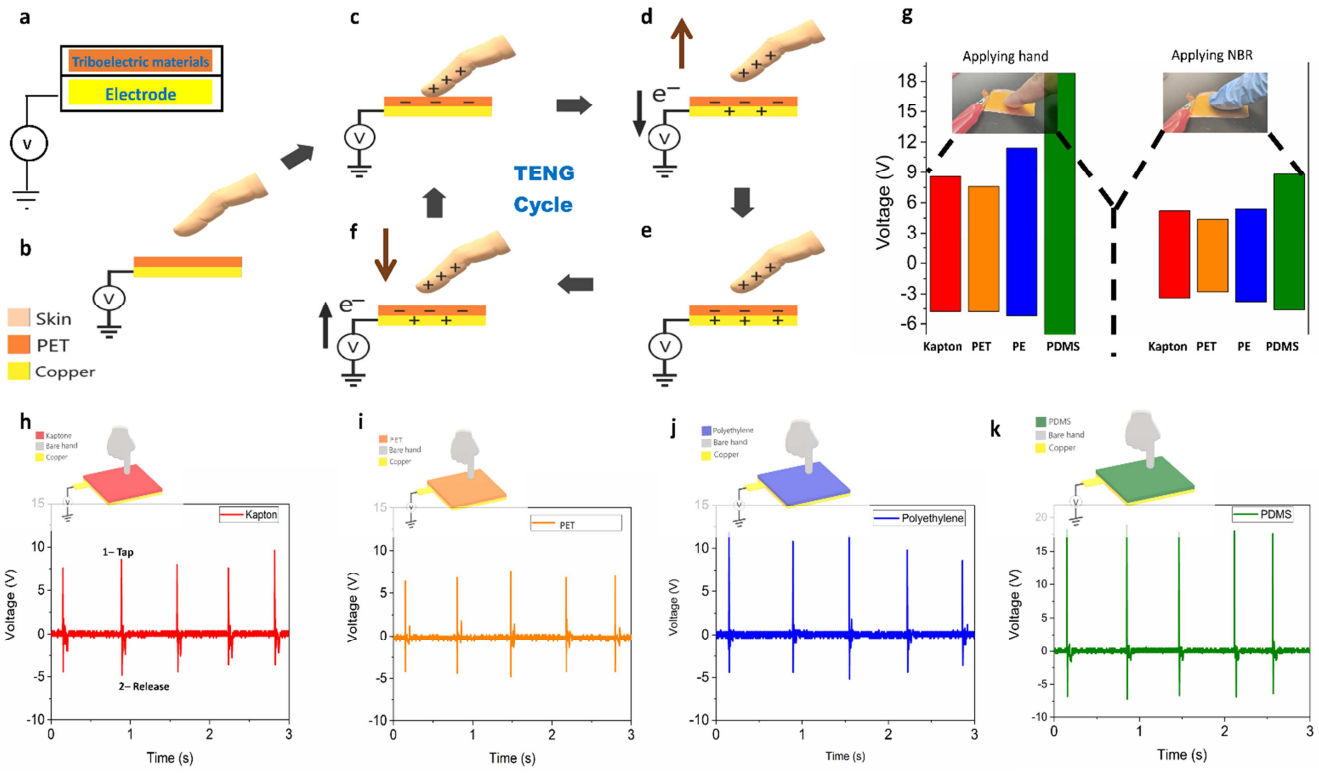

Figure 1: **(a)** Single Electrode Triboelectric Nanogenerator for primary testing. Working Mechanism: **(b)** Initial stage of the TENG, **(c)** Full contact with the finger, **(d)** Finger released from the TENG, **(e)** Full separation from the TENG, **(f)** Finger moving towards the TENG, **(g)** Maximum peak to peak voltage observed applying hand and NBR for different materials. Voltage observed applying hand with **(h)** Kapton, **(i)** PET, **(j)** Polyethylene (PE), and **(k)** Polydimethylsiloxane (PDMS).

Testing the triboelectric output for finger tapping with different materials

Finger 1a shows a single electrode triboelectric nanogenerator (SETENG) which was fabricated to test the triboelectric effect due to finger tapping motion with different materials and select proper material for the energy case. The testing device was basically consisted of a layer of testing material and a Copper electrode. The test was run by applying tapping motion on the device with bare fingers and NBR covered fingers. Human skin and NBR has low affinity for surface electron according to the triboelectric series [36,54]. To obtain higher triboelectric effect with finger and NBR , the testing materials were selected considering their lower position in the triboelectric series[55]. Hence, Kapton (Polyimide), Polyethylene tetraphthalate (PET), Polyethylene(PE) and Polydimethylsiloxane(PDMS) were used as the materials for primary testing due to the position in the triboelectric series [22,54,56,57].

The working principle of the single electrode triboelectric nanogenerator using tapping motion between finger and PET was explained through figure 1b to 1f. The mechanism can be explained as a combination of contact triboelectrification and electrostatic induction [3,58] Figure 1b shows the initial position of the finger which is kept at a certain distance from the SETENG. When tapping operation is started the finger gets in contact with the PET layer (Figure 1c). Due to the higher surface charge affinity of PET electron transfers from the skin to the PET layer resulting contact triboelectrification between these two surfaces [3,36,54,57,59,60]. As the finger starts separating from the PET layer, electrons start moving to the ground from the Cu electrode

to compensate the effect of contact triboelectrification of the PET surface (Figure 1d). An output voltage signal can be observed at the output due to this effect of electrostatic induction. Eventually, the electron stops flowing after the complete separation of these two layers as the electrons of the PET surface gets balanced by the induced positive charges of the electrode (Figure 1e). No output voltage can be observed at this stage. The finger starts moving towards the PET layer again (Figure 1f). As the positive charges on the finger gets closer to the PET surface, the electrons start moving to the electron to maintain the charge balance resulting a reversed output voltage. This cycle continues until the tapping motion is stopped. This mechanism is applicable for Kapton, PE and PDMS as well.

The primary testing was performed at 90 BPM (1.5Hz) tapping frequency keeping 3 cm as the distance between the index finger and the testing materials. The results showed different reading of open circuit voltage for different testing materials. Figure 1g demonstrates the maximum peak to peak voltage obtained from the SETENG for tapping motion with bare and gloved index finger on Kapton, PET, PE and PDMS film. Besides, figure 1h-k demonstrates the output voltage signal for tapping kapton, PET, PE and PDMS respectively with bare fingers for 3s time interval. With the application of stress with finger the output voltage rises to the maximum point 1(Figure 1h). However, the direction of the electron flow changes with the release of pressure resulting reversed output voltage which reaches up to point 2 (Figure 1h). Point 1 and point 2 can be defined as the maximum and the minimum peaks of voltage. It is clear from the figures that the PDMS film showed highest triboelectric output by interacting with the bare finger compared to the other materials. The PDMS-finger interaction generated a highest voltage of 18.8V and a peak to peak voltage of 7.2V (Fig 1g and 1k). However, kapton, PET and PE also showed decent response with the finger which generated highest output voltage of 8.6 V

(Fig 1h), 7.6 V (Fig 1i) and 11.5V (Fig 1j) and peak to peak voltage of 13.4 V, 12.4 V and 16.7 V (Fig 1g), respectively. According to the triboelectric series the PDMS has the higher electron affinity compared to kapton, PET or PE [22]. This higher affinity of electron leads towards higher triboelectric output due to the interaction with bare fingers. On the other hand, it was also observed that tapping motion with bare fingers produced compared to the fingers with NBR gloves (Fig 1g). The maximum open circuit voltage and peak to to peak voltage using the NBR-PDMS interaction was observed to be 8.8V and 13.4V respectively. Besides, the maximum peak to peak voltage for kapton, PET and PE was measured to be 8.6V, 7.3V and 9.2V respectively. The NBR has lower position compared to the human skin according to the triboelectric series. It has a charge affinity of +3nC/J which is quite low compared to the charge affinity of human skin(+30nC/J) [54]. Hence, it exhibits lower triboelectric effect than the human skin. The results of the primary testing clearly shows the prospect of using finger taping to generate electricity with kapton, PET, PE and PDMS.

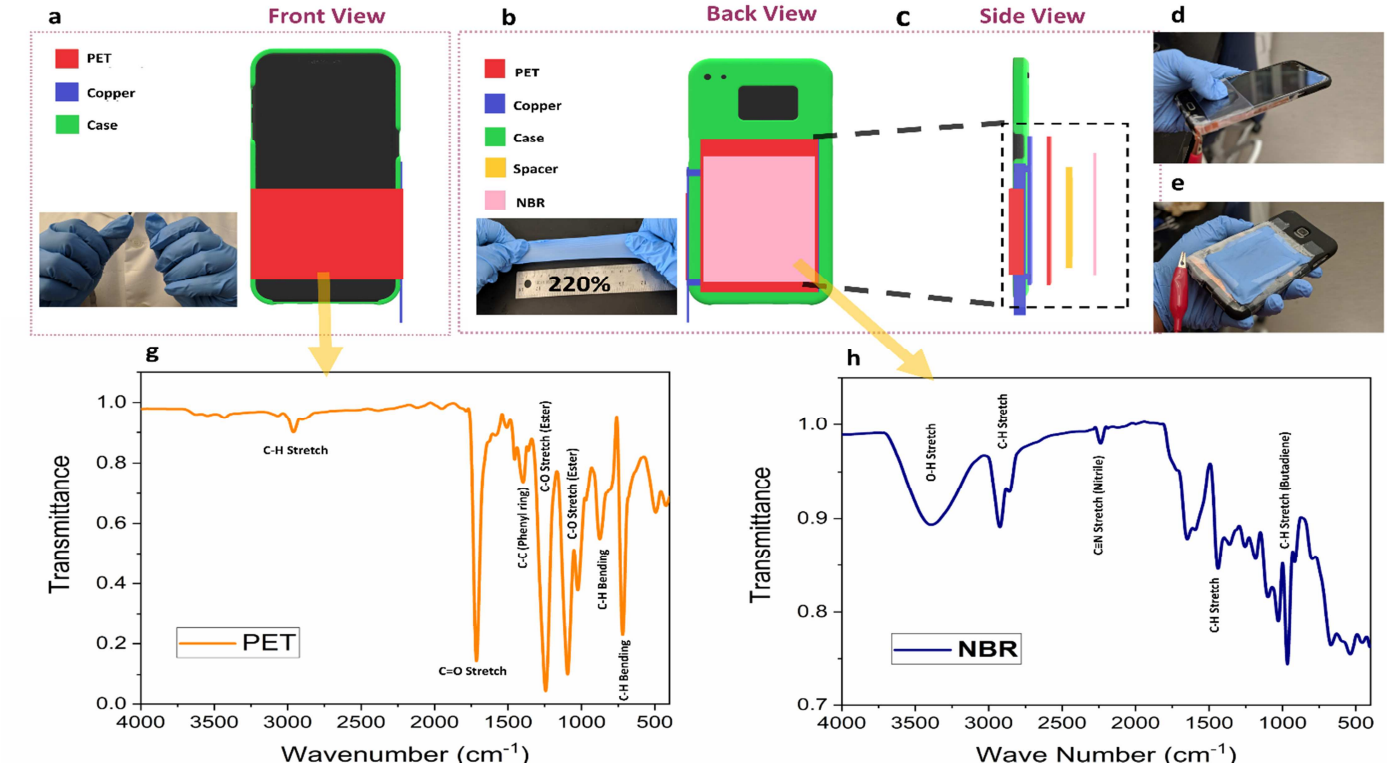

Figure 2: **(a)** Front view (inset: transparent PET films), **(b)** Back view (inset: Highly stretchable NBR films), and **(c)** Side view of the mobile attached TESTEC schematic. **(d)** Front part an, **(e)** back part of the optical view of the TESTGC. Fourier-transform infrared spectroscopy (FTIR) spectra of **(f)** PET film and **(g)** NBR film.

Triboelectricity based Stepping and Tapping Energy Case (TESTEC): Materials and Characterization

Touch electronic devices has become an integral part of everyday life of a big portion of World's population. According to Dscout research firm, a touch phone is on average being touched about 2617 times by a person everyday [61]. To utilize the mechanical energy from touching motion a Triboelectricity based Stepping and Tapping Energy Case (TESTEC) was built based on the results of the primary testing discussed in the previous section. The front part of the TESTEC consists of a rectangular shape transparent PET film and a Copper electrode which attached with the PET film (Fig 2a). PET showed good triboelectric response during the

interaction with hand and NBR discussed in the previous section. These cost effective thermoplastic have been widely used as touch screen protector due to its high strength, transparency and light weight as well as resistance to impact, shatter and scratch [62–64]. On the other hand, the back part includes a PET and NBR film separated by air gap with the help of a rectangular shaped spacer foam. A Copper film is attached with the PET film which works as an electrode. Figure 2b and 2c demonstrates the back and side view of the TESTEC respectively. NBR is a highly flexible and cost effective polymer [65,66]. It showed good triboelectric response while examining interaction between PET film and NBR gloves mentioned in the previous section. The front and back part of the TESTEC was designed to utilize mechanical energy directly from finger tapping and indirectly from foot stepping.

The characterization of the PET and NBR film was performed through Fourier Transformation Infrared (FTIR) Spectroscopy using Attenuated Total Reflection (ATR) technique. Figure 2d provides graphical demonstration of FTIR spectra of the PET film from 400 to 4000 cm^{-1}. The asymmetric sharp peak at 1095 cm^{-1} and the symmetric sharp peak at 1243 cm^{-1} are due to the C-O stretch of Este. Besides, the peak at 1394 cm^{-1} comes from the vibration of C-C from the phenyl ring. Also, the sharp peak at 719 cm^{-1} denotes C-H bending from the out of plane benzene group. Furthermore, the C=O stretch resulted a sharp peak at the wavelength of 1714 cm^{-1} [67–70]. On the other hand, figure 2e shows the FTIR spectra of the NBR film. The peak at 2237 cm^{-1} confirms the presence of nitrile group (C≡N). Also, the peak at 966 cm^{-1} corresponds the C-H stretch from Butadiene group. Besides, the peaks at 1440 cm^{-1} and 2923 cm^{-1} attributes to the C-H stretch of NBR rubber [71,72].

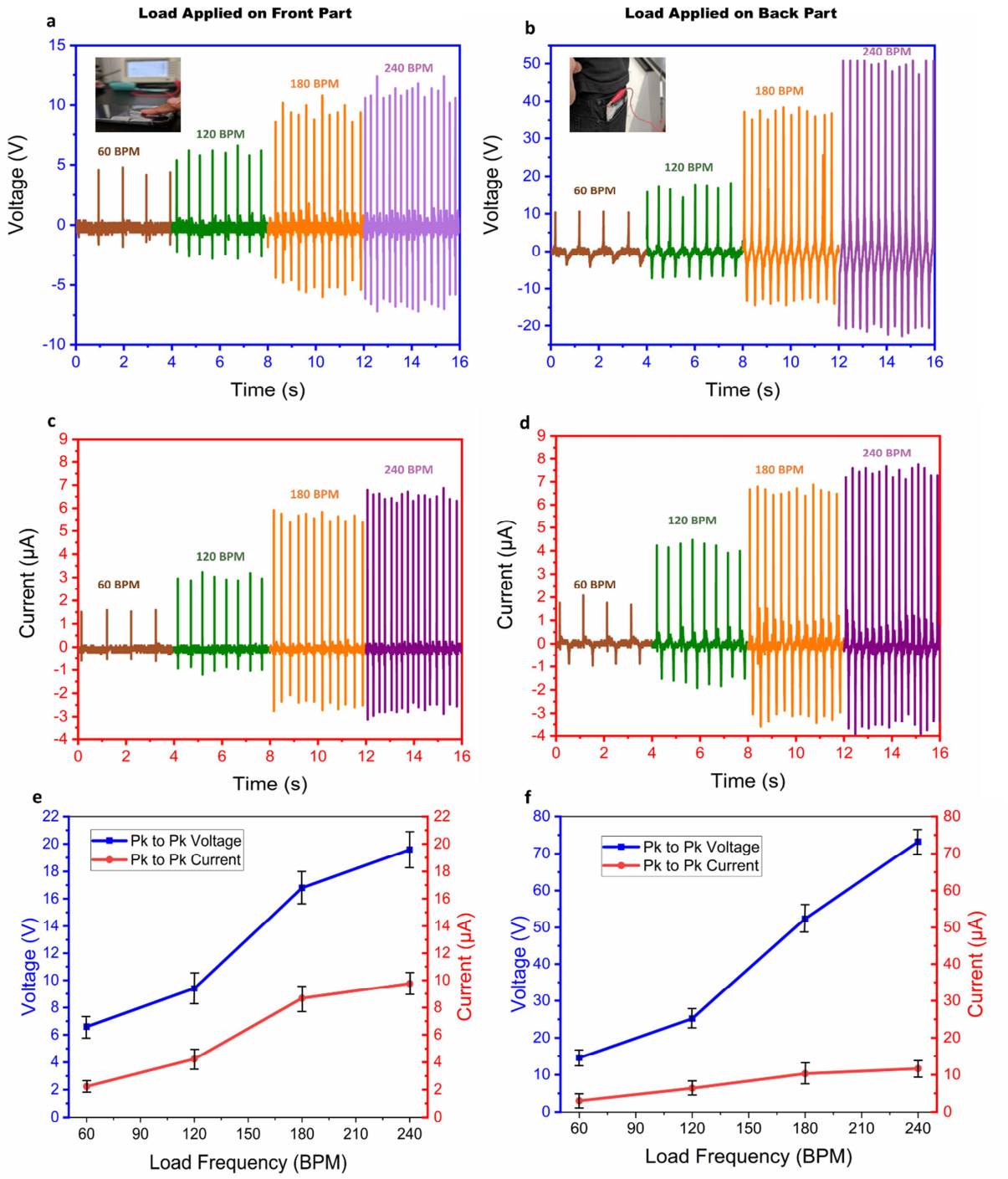

Figure 3: Voltage observed for different load frequency on **(a)** front part (inset: Device during tapping on the front part) and **(b)** back part (inset: Device during stepping). Current observed for different load frequency on **(c)** front part and **(d)** Back part. Comparison of maximum peak to peak voltage and current observed for **(e)** front part and **(f)** back part with error bars (Standard deviation for 3 readings)

Output performance of TESTEC under variable frequency, air gap and fingertip combinations

The output characterization of TESTEC was performed under variable load frequency. The front part of the device was tapped with the index finger at 60 BPM (1Hz), 120 BPM (2Hz), 180 BPM (3Hz) and 180 BPM (4Hz) frequencies keeping 3cm surface gap (Fig 3a inset). Also, the back part was tested by stepping at the same frequencies maintaining 5cm surface gap between the shoe sole and the floor while the device was set at the pocket (Fig 3b inset). The supplementary movie 1 and 2 demonstrates the tapping and stepping test of the TESTEC at 120 BPM. The stepping motion results in movement of the thigh which vertically pushes the back part of the TESTEC and creating triboelectric effect. Figure 3a and 3b shows the open circuit voltage at output recorded at variable load frequency for the front and the back part of the TESTEC respectively. On the other hand, Figure 3c and 3d demonstrated the short circuit current at output for the same load condition. The maximum output voltage observed for the front part was 4.8, 6.6, 10.7 and 12.4 V (Fig 3a) for 60, 120, 180 and 240 BPM load frequencies respectively. Besides, the corresponding maximum output currents were 1.6, 3.2, 5.9 and 6.9 μA (fig 3b). The impact velocity increases parallelly with load frequency. As a result, the electrons in the external circuit gets shorter time to neutralize the triboelectric potential leading towards a larger flow of electron [3,73–75]. Hence, the increment in the frequency leads towards larger current. Correspondingly, the output voltage increased with the increase of current as voltage is a linear function of the current [74,75]. However, the back part showed higher output response due to the stepping motion. The maximum output voltage for the back part were recorded as 10.6, 17.8, 38.4 and 50.8V whereas the currents were 2.08, 4.48, 6.88 and 7.76μA respectively. PET showed higher response with human skin compared to the NBR in the primary experiment

278 discussed above. However, the back part of the device involved higher surface area(54cm^2) in
279 the triboelectric action between the NBR and PET The finger tapping on the front part only
280 involved the surface area about 6.67cm^2 (index finger tip volar) [76]. The higher surface area
281 resulted higher charge transfer between the surfaces leading towards higher triboelectric output
282 of the back part [9,77]. But the front part showed higher output based on current density.
283 Compared to the maximum current density of 0.14 $\mu A/cm^2$ of the back part at 240 BPM, the
284 front part exhibited a maximum current density of 1.03 $\mu A/cm^2$. Figure 3e and 3f demonstrates a
285 graphical representation of maximum peak to peak output voltage and current observed at
286 variable load frequency for the front and back part respectively. The peak to peak current and
287 voltage increased linearly for both parts with increasing frequency. However, the rate of this
288 increase is lower for the peak to peak current of the back part which is promoted due to the
289 higher resistivity of NBR compared to human skin [78,79].

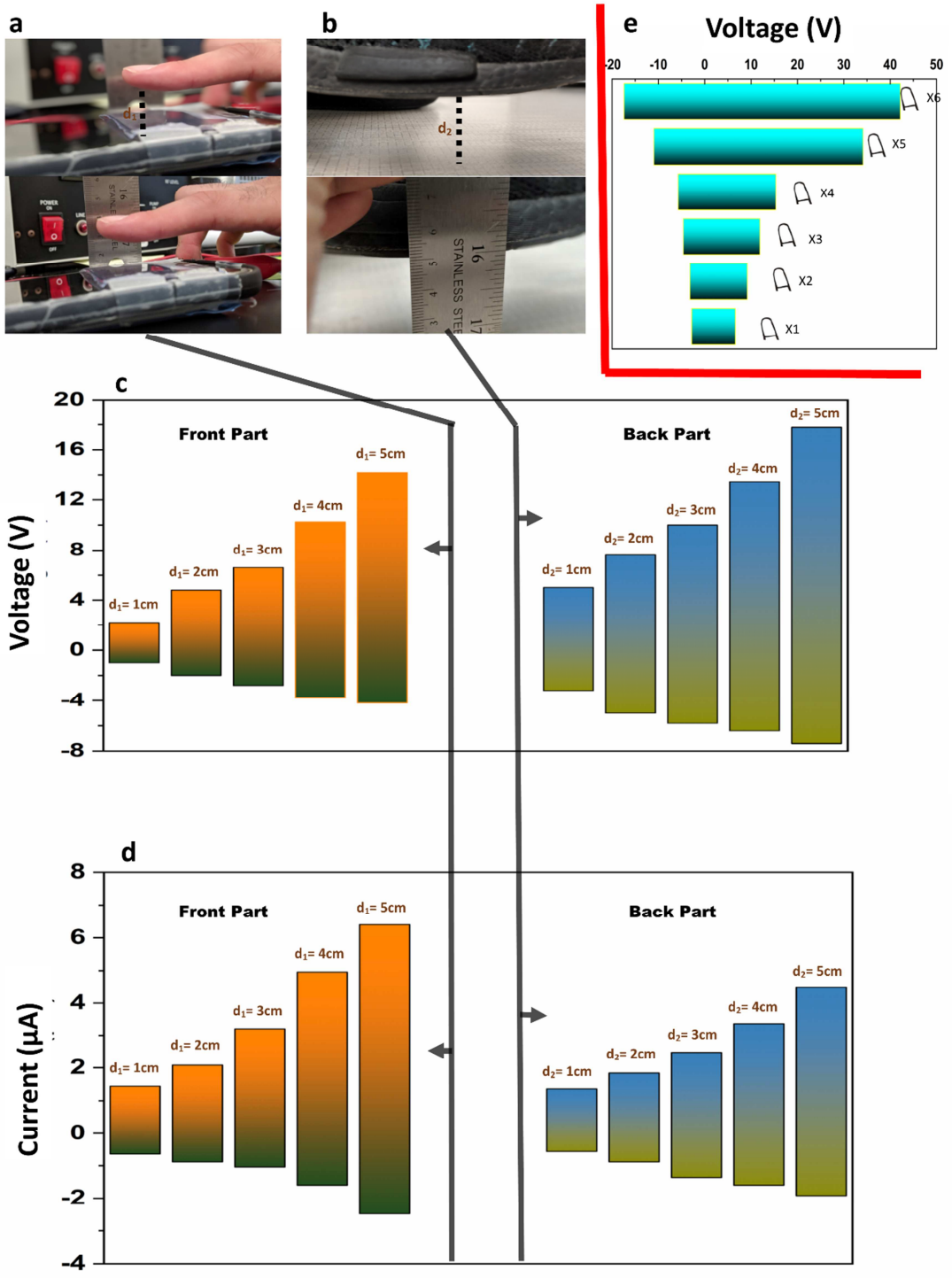

Figure 4: **(a)** Tapping and **(b)** Stepping Test at variable distance. **(c)** Observed voltage at variable distance for the front and back part. **(d)** Observed current at variable distance for the front and back part. **(e)** Observed maximum voltage at variable fingertip combination

The output performance of the TESTEC was also tested for variable air gap between the operating surfaces. The test was performed at 120 BPM tapping and stepping frequency with a variable airgap from 1 to 5 cm for the front (Figure 4a) and back (Figure 4b) part respectively. As the airgap increased from 1cm to 5 cm, the voltage increased linearly from 2.2 to 14.2 V for the impact on the front side as well as from 5 to 17.8 V for the impact on the back side (Figure 4c). As the airgap increases, the force due to the impact on the triboelectric surface also increases directly for the front side and indirectly for the back side. Since the frequency of tapping is kept constant, the velocity of the finger increases with increased airgap. So, the momentum increases with the increased velocity concluding towards higher force of impact. This magnified force leads to larger deformation of the contact surface of the triboelectric layers resulting higher surface area and higher output voltage [74,80,81]. The output current also increased linearly with increasing airgap. While the maximum output current was observed as 1.5 µA for the front part at 1cm airgap, the output current increased to 6.4 µA at 5 cm airgap. Likewise, The output current increased from 1.3 to 4.5 µA for the back part. As discussed before, the velocity of the finger increases due to the increased airgap with constant frequency of impact. So, The kinetic energy on the triboelectric layer increases with the increase of velocity which leads towards larger transfer of electrons through the triboelectric surfaces [74,80]. As a result, electrons from the electrodes flow at a higher rate to neutralize the larger transfer of electrons of the triboelectric surfaces which results higher output current in the output.

The output performance of TESTEC was further tested by tapping with multiple fingers. The front part of the device was tapped at 3 cm airgap and 120 BPM frequency using different combination of fingertip. The volar section of the index, middle and ring fingers of both hands

were used for this test. Figure 4e demonstrates maximum peak to peak voltage obtained for variable fingertip combination at the output. The maximum peak to peak voltage using the index fingertip was 9.4 V. As the middle finger was added with the index finger the peak to peak voltage increased to 12.3 V. The surface area of the contact triboelectrification increased from 6.67 cm^2 to 13.84 cm^2 when the middle fingertip was added with the index finger [76]. The higher surface area of the combined index and middle fingertip promoted higher triboelectric output [9,82]. The highest peak to peak voltage was obtained for the combination of index, middle and ring fingertip of both hands (59.6 V). However, the output signal did not rise linearly due to the unequal surface area as well as variation of impact of the fingers. When the index finger of the left hand was added with the other three fingers (index, middle and ring fingers) of the right hand, the output signal increased exponentially as the index finger of the left hand created higher impact combining with the other three fingers of the right hand.

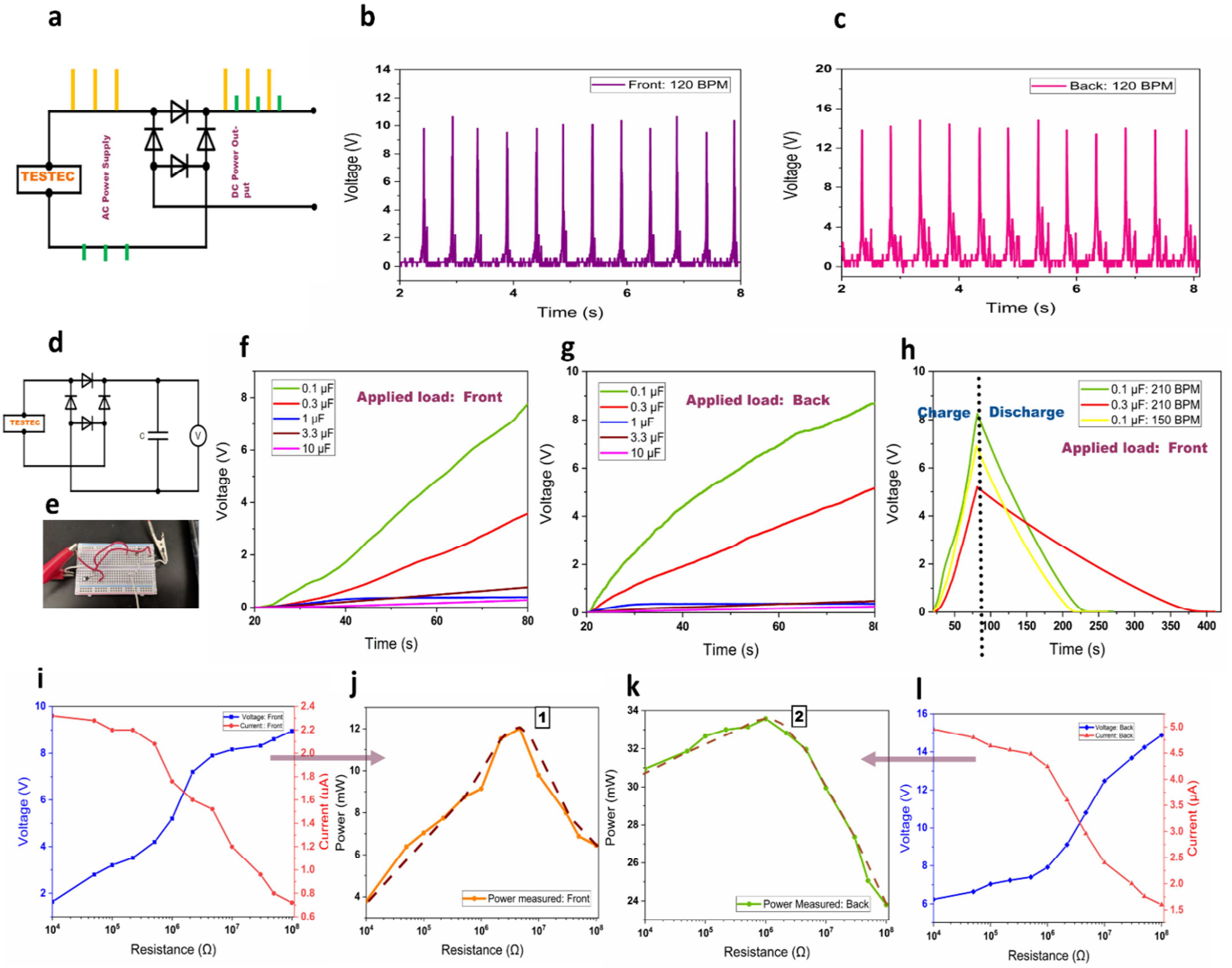

Figure 5: **(a)** Circuit diagram for rectifying the signals by TESTEC. Rectified voltage signal at 120 BPM load frequency for **(b)** front part and **(c)** back part. **(d)** Schematic circuit diagram and **(e)** Optical view of circuit diagram for charging and discharging capacitors with TESTEC. Charging capacitors of variable capacitance for 60 seconds by applying load on the **(f)** front part and **(g)** the back part of the TESTEC. **(h)** Ability of the TESTEC to charge and capacitors for different load frequencies by applying load on the front part. **(i)** Average voltage and current measured at variable external resistance with front part of the TESTEC. **(j)** Average power measured by applying load on the front part of the TESTEC at different external resistances. **(k)** Power measured by applying load on the front part of the TESTEC at different external resistances. **(l)** Average power measured by applying load on the back part of the TESTEC at different external resistance.

Integration of The TESTEC with conventional electronic components

The output performance of the TESTEC was also tested with conventional electronic components. Firstly, the output response of TESTEC was studied by integrating with a full wave bridge rectifier. Figure 5a demonstrates the equivalent circuit diagram for converting the AC power signal to DC signal. Figure 5b and 5c shows the full wave rectified voltage signal obtained from tapping the front and back part of the device at 120BPM frequency and 5cm airgap respectively. The maximum output rectified open circuit voltage was recorded as 10.6 and 14.8V for the front and back part respectively. Point 1 and 2 from figure 5b shows the rectified output signal due to tapping and releasing on the front part respectively while the point 3 and 4 from figure 5c shows it for step down (press) and step up (release) motion operating the back part. The output signal from releasing operation is quicker for the front part compared to the back part as the direct contact and release of the front part results quicker separation between contact surfaces compared to the indirect contact and release of the back part.

After examining the device with the full bridge rectifier, the device was examined with capacitor to test the prospect of storing energy from the tapping and stepping motion as well as providing constant bias voltage to power touch based electronic equipment [80,83]. Figure 5d and 5e demonstrates schematic and optical view of the equivalent circuit diagram where the device was integrated with a full bridge rectifier and a capacitor. Capacitors of 0.1, 0.3, 1, 3.3 and 10 µF were used for the test at 5cm airgap. Figure 5f and 5g shows the open circuit voltage for charging the capacitors for 60 seconds at 210 BPM frequency using the front and back part of the TESTEC respectively. The higher the capacitance of the capacitor, the lower the rate of charging. For instance, the output voltage observed for 0.1 µF was 7.7 V which was 3.6 V for 0.3 µF capacitor after charging it for 60 s using the front part. Similarly, the discharge rate was higher for the 0.1 µF capacitor. It took 145 s for discharging the 0.1 µF capacitor completely

where it took 302 s for the 0.3 µF capacitor (Figure 5h). In case of the back part, the output voltage with the capacitors of 0.1 and 0.3 µF was measured as 8.7 and 5.2 V respectively. The 0.3 µF capacitor charges slower than the 0.1 µF capacitor due to the higher loss of charges in the capacitor [80,83,84]. In addition, the output voltage of the front part with the 1, 3.3 and 10 µF capacitors were observed to be 0.78, 0.4 and 0.29 V respectively after charging the capacitors for 60s. Likewise, this output voltage was 0.38, 0.49 and 0.25 V for the back part. Furthermore, the effect of variable frequency was observed for charging and discharging the 0.1 µF capacitor with the front part of the TESTEC (Figure 5h). The rate of charging at 210 BPM was higher than 150 BPM. As the number of contacts is larger in case of 210 BPM frequency, larger number of charges transfer from the finger to the PET film during charging operation. Hence, higher output voltage can be obtained which results higher rate of charging. However, the rate was observed to be lower for 210 BPM in case of discharging. Due to the accumulation of higher voltage during charging operation, it takes more time for discharging the capacitor at 210 BPM tapping frequency. The energy conversion efficiency was measured based on the output energy from the capacitor test. The input energy was ideally considered to be the initial potential energy from the finger and the foot in 5cm height. The maximum energy conversion for 0.3µF capacitor was calculated to be 57.4% for the front part and 4.46% for the back part. The direct impact on the PET layer from the finger resulted in higher efficiency of the front part of the device. On the other hand, the back part was driven indirectly by the contact between the foot and the floor which resulted intermediate loss of energy and lower energy conversion efficiency.

The output power, voltage and current of the TESTEC were also characterized with external loads from 10^4 to 10^8 Ω for both parts. With the increase of the resistance the output voltage rises while the output current decreases following the Ohm's law (Fig 5i and 5l).

Nevertheless, a sharper increment of the voltage can be observed from 0.25 and 0.5 MΩ resistance for front and back part correspondingly. This inverse tends of the output voltage and current leads towards the measurement of power at optimum resistance. Figure 5j and 5k shows Power measured for the front part and the back part respectively. The corresponding maximum power obtained from the TESTEC was 12.1 mW (3.78 mW/m^2) at 0.46 MΩ for the front part and 33.56 mW (6.21 mW/m^2) at 1.02 MΩ for the back part.

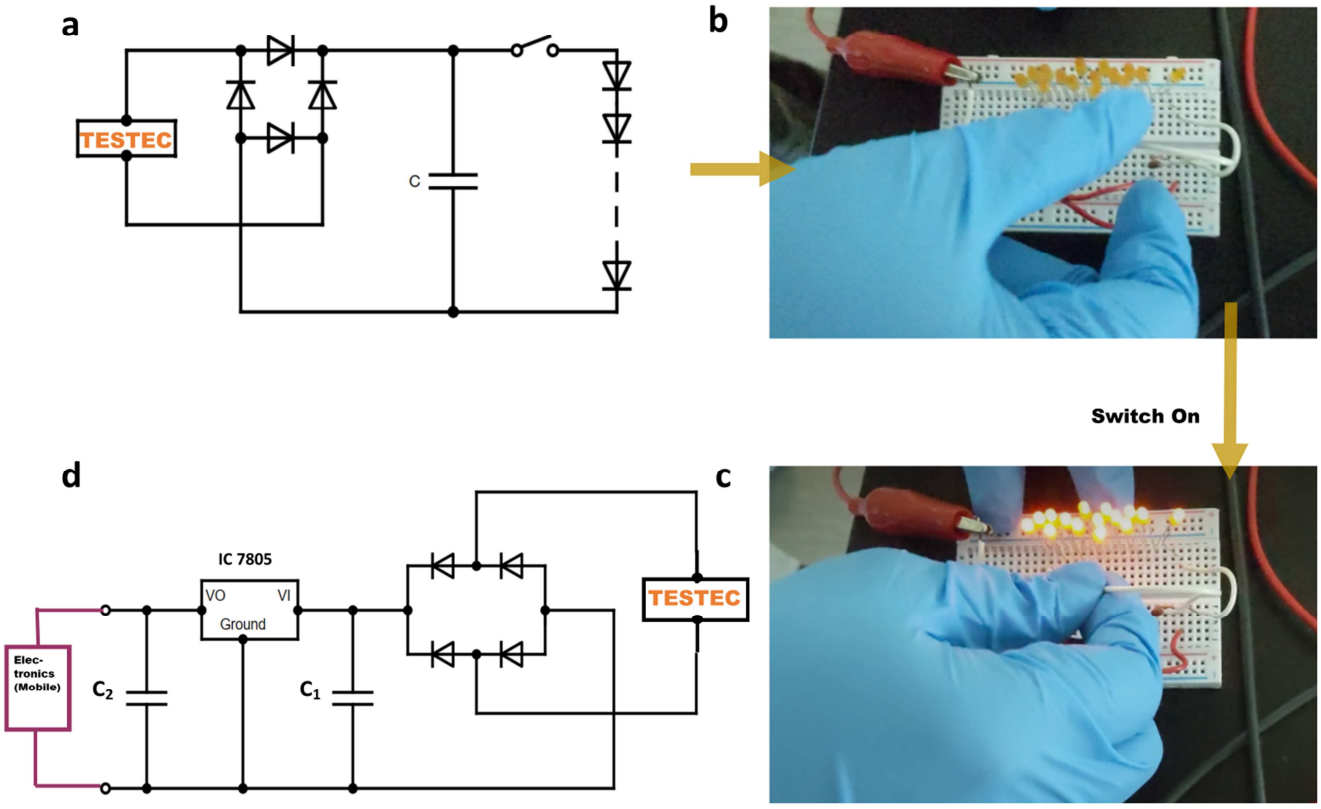

Figure 6: **(a)** Circuit diagram for powering LED's with TESTEC. **(b)** Switch off mode of the circuit. **(c)** Lighting 15 LEDs with the TESTEC. **(d)** Proposed Circuit diagram for charging electronics (mobile phone).

Powering smart electronics with TESTEC

In the previous sections, energy harvesting and storing capability of the TESTEC has been discussed at different conditions. For further application, we investigated the TESTEC for lighting commercial Light Emitting Diodes (LED). Figure 6a shows equivalent circuit diagram for lighting commercial LEDs with TESTEC. A series of LEDs were attached with a capacitor and a full bridge rectifier. The front part of the TESTEC was switched off and tapped at 120 BPM frequency for 60 seconds (Figure 6b). After switching on the circuit, 15 commercial LEDs were lightened with the TESTEC (Figure 6c). The output of the LED test as well as the capacitor test magnify the prospect of the TESTEC for the application of powering smart electronic devices [26,37,60]. For instance, Most of the smart phone now a days are run by Li-ion batteries which usually operates between 1.5 to 4.2 V [85,86]. The tapping and stepping motion can be applied to partially charge these batteries. An equivalent simple circuit diagram is proposed at figure 6d to charge smart electronics with TESTEC. An IC 7805 can be used for regulating the voltage at 5 V [87]. Two capacitor C1 and C2 are used to remove AC ripples and maintain proper voltage supply at the output. Utilizing the tapping and stepping motion through TESTEC will reduce energy loss thus promoting sustainability.

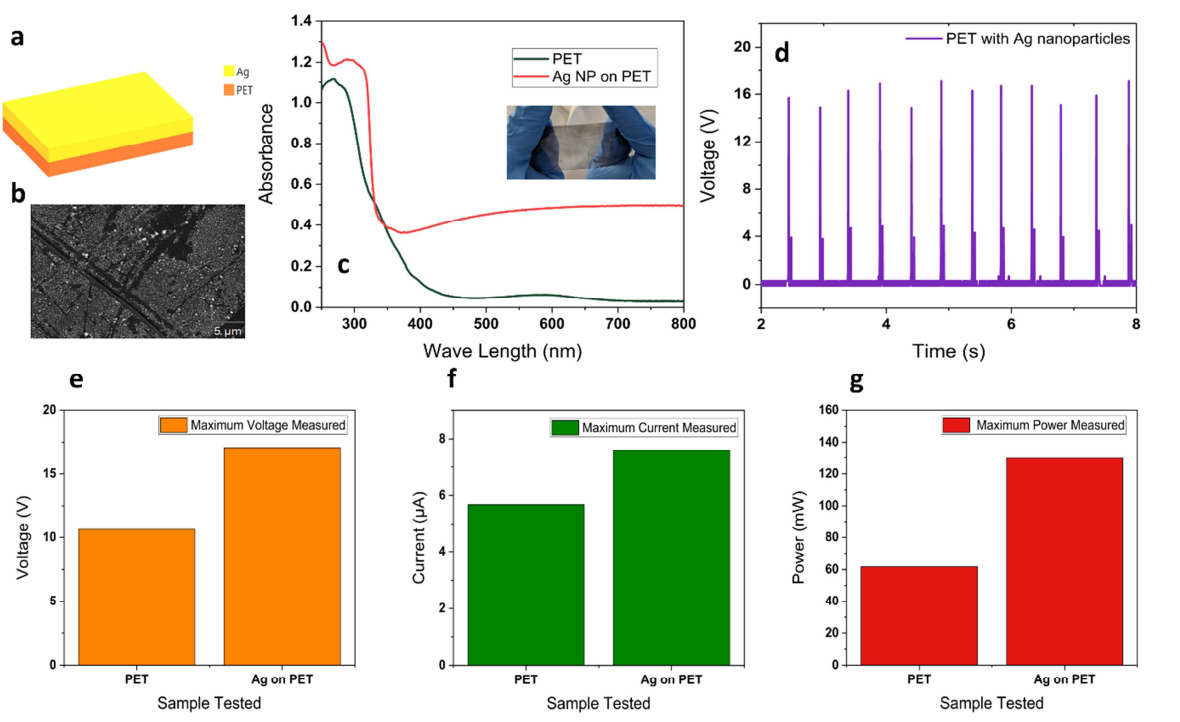

Figure 7: **(a)** Ag nanoparticles over PET film. **(b)** SEM image of Ag sputtered PET film for the modified TESTEC. **(c)** Ultraviolet–visible (UV) Vis Spectra of PET film with and without Ag nanoparticles. (inset: Optical view of the Ag sputtered PET fim) **(d)** Rectified voltage signal by the modified TESTEC at 120 BPM load frequency. **(e)** Comparison between maximum rectified voltages obtained from standard and modified TESTEC. **(f)** Comparison between maximum rectified current obtained from standard and modified TESTEC. **(g)** Comparison between maximum rectified power obtained from standard and modified TESTEC.

Modification of TESTEC: Application of Ag Nanoparticle

To obtain performance from the TESTEC Ag nanoparticle were used on the PET film. A very thin layer(10nm) of Ag nanoparticles were sputtered on the PET film (Figure 7a). Application of Ag nanoparticles leads to higher contact surface in triboelectric operation compared to the plain surface [88]. Although Ag nanoparticles slightly effects the transparency of the PET layer, PET layer works as a base which holed the Ag layer. Besides, the mechanical properties of the PET can be sustained during the operation of TESTEC. Figure 7b shows the

SEM image of the PET layer sputtered with Ag nanoparticles. The image provides a clear view of Ag nanoparticles on the PET film. The UV-Vis spectra was used for characterizing the optical properties of the Ag/PET film [89]. Figure 7c shows the UV-Vis spectra of Ag particle-deposited PET film and commercial PET film. The maximum absorbance of the commercial PET film was observed at 266nm wavelength. However, the spectra deviated with higher absorbance for the Ag based PET film due to the presence of Ag nanoparticles[89–91]. The inset of figure 7c shows the optical view of the PET film, sputtered with Ag nanoparticles for the modified TESTEC.

The modified PET film was attached with the TESTEC for examining its triboelectric response and compared with the measured values of the plain PET surface as well. The modified TESTEC was tapped at 120 BPM with an airgap of 5cm. The results showed a higher triboelectric response due to the application of Ag nanoparticles. The maximum rectified voltage was observed to be 17.1 V (Figure 7d) which on the other hand was 10.6 V for the plain PET surface (Figure 7e). Also, the maximum output current and power were increased by 2 μA and 68.1 mW for the modified TESTEC, respectively (Figure 7f and 7g). This enhanced surface area of the modified TESTEC resulted higher output response due to the higher charge transfer in the surface. But, this enhancement was depleted as the triboelectric response was basically observed due to the interaction between Ag and skin which has less gap in triboelectric series compared PET and skin [54,57]. Modification of the TESTEC showed the prospect of scavenging more energy compared to the standard TESTEC.

Conclusion

In summary, we have designed a cost effective and adjustable energy case (TESTEC) with commercial PET and NBR films to harvest mechanical energy through triboelectric mechanism. It was designed to adjust with touch electronic devices and power them directly from tapping and stepping motion while using and carrying the electronic devices. The TESTEC successfully converted mechanical energy into electrical energy in which the output response by the device was increased linearly with increased frequency and airgap during tapping and stepping operation. The maximum output voltages of the front and back parts were measured as 14.8 and 50.8 V, respectively. Also, the output voltage raised up to 59.1 V when the front part was tapped with 6 fingers altogether. Further development of the TESTEC can be conducted for increasing the output current. In addition, the TESTEC showed an excellent response when it was integrated with capacitors, resistors and bridge. Also, it was successfully applied for charging capacitors and driving commercial LEDs rectifier which amplifies its prospect in utilizing mechanical energy through electrical energy. Furthermore, the modification of the TESTEC with Ag nanoparticles resulted higher output response. The output power was increased by 68.1 mW due to the application of Ag nanoparticles on the TESTEC. In future, the TESTEC can be tested with other nanoparticles like Au, Si and Cu as well for further development. Besides, the front part can be investigated with materials like polyurethane, tempered glass and Polypropylene for better outputs. This device holds a lot of potential for utilizing recyclable plastics from the environment. It has the potential to reduce the necessity of charging smart electronic devices through usual procedures. Promoting the TESTEC in industrial level will also promote renewable energy and sustainable development.

Acknowledgement

The authors would like to acknowledge the support of the Graduate College, University of Texas Rio Grande Valley to Abu Musa Abdullah through Presidential Graduate Research Assistantship. This research was supported by National Science Foundation (NSF PREM) award under grant No. DMR-1523577: UTRGV-UMN Partnership for Fostering Innovation by Bridging Excellence in Research and Student Success. This project was partially supported by the Welch Foundation Award: BX-0048.

References

[1] E. Ozdalga, A. Ozdalga, N. Ahuja, The Smartphone in Medicine: A Review of Current and Potential Use Among Physicians and Students, Journal of Medical Internet Research. 14 (2012) e128. https://doi.org/10.2196/jmir.1994.

[2] Technology in Our Life Today and How It Has Changed | Updated for 2019, AgingInPlace.Org. (2018). https://www.aginginplace.org/technology-in-our-life-today-and-how-it-has-changed/ (accessed August 26, 2019).

[3] A.R. Chowdhury, A.M. Abdullah, I. Hussain, J. Lopez, D. Cantu, S.K. Gupta, Y. Mao, S. Danti, M.J. Uddin, Lithium doped zinc oxide based flexible piezoelectric-triboelectric hybrid nanogenerator, Nano Energy. 61 (2019) 327–336. https://doi.org/10.1016/j.nanoen.2019.04.085.

[4] N. Espinosa, M. Hösel, D. Angmo, F. C. Krebs, Solar cells with one-day energy payback for the factories of the future, Energy & Environmental Science. 5 (2012) 5117–5132. https://doi.org/10.1039/C1EE02728J.

[5] L. Lin, S. Wang, S. Niu, C. Liu, Y. Xie, Z.L. Wang, Noncontact Free-Rotating Disk Triboelectric Nanogenerator as a Sustainable Energy Harvester and Self-Powered Mechanical Sensor, ACS Appl. Mater. Interfaces. 6 (2014) 3031–3038. https://doi.org/10.1021/am405637s.

[6] M.S. Dresselhaus, I.L. Thomas, Alternative energy technologies, Nature. 414 (2001) 332–337. https://doi.org/10.1038/35104599.

[7] E. Koçak, A. Şarkgüneşi, The renewable energy and economic growth nexus in Black Sea and Balkan countries, Energy Policy. 100 (2017) 51–57. https://doi.org/10.1016/j.enpol.2016.10.007.

[8] A.M. Abdullah, A.R. Chowdhury, Y. Yang, H. Vasquez, H.J. Moore, J.G. Parsons, K. Lozano, J.J. Gutierrez, K.S. Martirosyan, M.J. Uddin, Tailoring the viscosity of water and ethylene glycol based TiO2 nanofluids, Journal of Molecular Liquids. 297 (2020) 111982. https://doi.org/10.1016/j.molliq.2019.111982.

[9] M. Ma, Z. Kang, Q. Liao, Q. Zhang, F. Gao, X. Zhao, Z. Zhang, Y. Zhang, Development, applications, and future directions of triboelectric nanogenerators, Nano Res. 11 (2018) 2951–2969. https://doi.org/10.1007/s12274-018-1997-9.
[10] F.-R. Fan, Z.-Q. Tian, Z. Lin Wang, Flexible triboelectric generator, Nano Energy. 1 (2012) 328–334. https://doi.org/10.1016/j.nanoen.2012.01.004.
[11] S. Wang, Z.L. Wang, Y. Yang, A One-Structure-Based Hybridized Nanogenerator for Scavenging Mechanical and Thermal Energies by Triboelectric–Piezoelectric–Pyroelectric Effects, Advanced Materials. 28 (2016) 2881–2887. https://doi.org/10.1002/adma.201505684.
[12] A.R. Chowdhury, J. Jaksik, I. Hussain, R. Longoria, O. Faruque, F. Cesano, D. Scarano, J. Parsons, M.J. Uddin, Multicomponent nanostructured materials and interfaces for efficient piezoelectricity, Nano-Structures & Nano-Objects. 17 (2019) 148–184. https://doi.org/10.1016/j.nanoso.2018.12.002.
[13] Y. Zi, L. Lin, J. Wang, S. Wang, J. Chen, X. Fan, P.-K. Yang, F. Yi, Z.L. Wang, Triboelectric–Pyroelectric–Piezoelectric Hybrid Cell for High-Efficiency Energy-Harvesting and Self-Powered Sensing, Advanced Materials. 27 (2015) 2340–2347. https://doi.org/10.1002/adma.201500121.
[14] R.K. Gupta, Q. Shi, L. Dhakar, T. Wang, C.H. Heng, C. Lee, Broadband Energy Harvester Using Non-linear Polymer Spring and Electromagnetic/Triboelectric Hybrid Mechanism, Scientific Reports. 7 (2017) 41396. https://doi.org/10.1038/srep41396.
[15] A.R. Chowdhury, J. Jaksik, I. Hussain, P. Tran, S. Danti, M.J. Uddin, Surface Modified Nanostructured Piezoelectric Device as Cost-Effective Transducer for Energy and Biomedicine, Energy Technology. 0 (n.d.). https://doi.org/10.1002/ente.201800767.
[16] C. Wu, A.C. Wang, W. Ding, H. Guo, Z.L. Wang, Triboelectric Nanogenerator: A Foundation of the Energy for the New Era, Advanced Energy Materials. 9 (2019) 1802906. https://doi.org/10.1002/aenm.201802906.
[17] S. Wang, L. Lin, Z.L. Wang, Triboelectric nanogenerators as self-powered active sensors, Nano Energy. 11 (2015) 436–462. https://doi.org/10.1016/j.nanoen.2014.10.034.
[18] F.-R. Fan, Z.-Q. Tian, Z. Lin Wang, Flexible triboelectric generator, Nano Energy. 1 (2012) 328–334. https://doi.org/10.1016/j.nanoen.2012.01.004.
[19] Z.L. Wang, J. Song, Piezoelectric Nanogenerators Based on Zinc Oxide Nanowire Arrays, Science. 312 (2006) 242–246. https://doi.org/10.1126/science.1124005.
[20] F. Yi, L. Lin, S. Niu, P.K. Yang, Z. Wang, J. Chen, Y. Zhou, Y. Zi, J. Wang, Q. Liao, Y. Zhang, Z.L. Wang, Stretchable-Rubber-Based Triboelectric Nanogenerator and Its Application as Self-Powered Body Motion Sensors, Advanced Functional Materials. 25 (2015) 3688–3696. https://doi.org/10.1002/adfm.201500428.
[21] F. Hu, Q. Cai, F. Liao, M. Shao, S.-T. Lee, Recent Advancements in Nanogenerators for Energy Harvesting, Small. 11 (2015) 5611–5628. https://doi.org/10.1002/smll.201501011.
[22] M.A.P. Mahmud, N. Huda, S.H. Farjana, M. Asadnia, C. Lang, Recent Advances in Nanogenerator-Driven Self-Powered Implantable Biomedical Devices, Advanced Energy Materials. 8 (2018) 1701210. https://doi.org/10.1002/aenm.201701210.
[23] Z. Lou, L. Li, L. Wang, G. Shen, Recent Progress of Self-Powered Sensing Systems for Wearable Electronics, Small. 13 (2017) 1701791. https://doi.org/10.1002/smll.201701791.
[24] Y. Zi, H. Guo, Z. Wen, M.-H. Yeh, C. Hu, Z.L. Wang, Harvesting Low-Frequency (<5 Hz) Irregular Mechanical Energy: A Possible Killer Application of Triboelectric Nanogenerator, ACS Nano. 10 (2016) 4797–4805. https://doi.org/10.1021/acsnano.6b01569.
[25] G. Zhu, Y.S. Zhou, P. Bai, X.S. Meng, Q. Jing, J. Chen, Z.L. Wang, A Shape-Adaptive Thin-Film-Based Approach for 50% High-Efficiency Energy Generation Through Micro-Grating Sliding Electrification, Advanced Materials. 26 (2014) 3788–3796. https://doi.org/10.1002/adma.201400021.

554 [26] W. Tang, T. Jiang, F.R. Fan, A.F. Yu, C. Zhang, X. Cao, Z.L. Wang, Liquid-Metal Electrode for High-
555 Performance Triboelectric Nanogenerator at an Instantaneous Energy Conversion Efficiency of
556 70.6%, Advanced Functional Materials. 25 (2015) 3718–3725.
557 https://doi.org/10.1002/adfm.201501331.
558 [27] E. Jovanov, A. Milenkovic, C. Otto, P.C. de Groen, A wireless body area network of intelligent
559 motion sensors for computer assisted physical rehabilitation, Journal of NeuroEngineering and
560 Rehabilitation. 2 (2005) 6. https://doi.org/10.1186/1743-0003-2-6.
561 [28] P.-J. (John) Hsu, Portable cell phone battery charger using solar energy as the primary source of
562 power, US6977479B2, 2005. https://patents.google.com/patent/US6977479B2/en (accessed
563 August 16, 2019).
564 [29] S. Niu, X. Wang, F. Yi, Y.S. Zhou, Z.L. Wang, A universal self-charging system driven by random
565 biomechanical energy for sustainable operation of mobile electronics, Nature Communications. 6
566 (2015) 8975. https://doi.org/10.1038/ncomms9975.
567 [30] Y. Wang, Y. Yang, Z.L. Wang, Triboelectric nanogenerators as flexible power sources, Npj Flexible
568 Electronics. 1 (2017) 10. https://doi.org/10.1038/s41528-017-0007-8.
569 [31] Y. Mao, N. Zhang, Y. Tang, M. Wang, M. Chao, E. Liang, A paper triboelectric nanogenerator for
570 self-powered electronic systems, Nanoscale. 9 (2017) 14499–14505.
571 https://doi.org/10.1039/C7NR05222G.
572 [32] X. Pu, L. Li, H. Song, C. Du, Z. Zhao, C. Jiang, G. Cao, W. Hu, Z.L. Wang, A Self-Charging Power Unit
573 by Integration of a Textile Triboelectric Nanogenerator and a Flexible Lithium-Ion Battery for
574 Wearable Electronics, Advanced Materials. 27 (2015) 2472–2478.
575 https://doi.org/10.1002/adma.201500311.
576 [33] J. Wang, X. Li, Y. Zi, S. Wang, Z. Li, L. Zheng, F. Yi, S. Li, Z.L. Wang, A Flexible Fiber-Based
577 Supercapacitor–Triboelectric-Nanogenerator Power System for Wearable Electronics, Advanced
578 Materials. 27 (2015) 4830–4836. https://doi.org/10.1002/adma.201501934.
579 [34] W. Liu, Z. Wang, G. Wang, G. Liu, J. Chen, X. Pu, Y. Xi, X. Wang, H. Guo, C. Hu, Z.L. Wang, Integrated
580 charge excitation triboelectric nanogenerator, Nature Communications. 10 (2019) 1426.
581 https://doi.org/10.1038/s41467-019-09464-8.
582 [35] X. Wang, B. Yang, J. Liu, Y. Zhu, C. Yang, Q. He, A flexible triboelectric-piezoelectric hybrid
583 nanogenerator based on P(VDF-TrFE) nanofibers and PDMS/MWCNT for wearable devices,
584 Scientific Reports. 6 (2016) 36409. https://doi.org/10.1038/srep36409.
585 [36] J. Xiong, P. Cui, X. Chen, J. Wang, K. Parida, M.-F. Lin, P.S. Lee, Skin-touch-actuated textile-based
586 triboelectric nanogenerator with black phosphorus for durable biomechanical energy harvesting,
587 Nature Communications. 9 (2018) 4280. https://doi.org/10.1038/s41467-018-06759-0.
588 [37] G. Zhu, P. Bai, J. Chen, Z. Lin Wang, Power-generating shoe insole based on triboelectric
589 nanogenerators for self-powered consumer electronics, Nano Energy. 2 (2013) 688–692.
590 https://doi.org/10.1016/j.nanoen.2013.08.002.
591 [38] Y.H. Ko, G. Nagaraju, S.H. Lee, J.S. Yu, PDMS-based Triboelectric and Transparent Nanogenerators
592 with ZnO Nanorod Arrays, ACS Appl. Mater. Interfaces. 6 (2014) 6631–6637.
593 https://doi.org/10.1021/am5018072.
594 [39] Q. Liang, X. Yan, Y. Gu, K. Zhang, M. Liang, S. Lu, X. Zheng, Y. Zhang, Highly transparent triboelectric
595 nanogenerator for harvesting water-related energy reinforced by antireflection coating, Scientific
596 Reports. 5 (2015) 9080. https://doi.org/10.1038/srep09080.
597 [40] Transparent Flexible Graphene Triboelectric Nanogenerators - Kim - 2014 - Advanced Materials -
598 Wiley Online Library, (n.d.). https://onlinelibrary.wiley.com/doi/full/10.1002/adma.201400172
599 (accessed July 26, 2019).

[41] K.Y. Lee, M.K. Gupta, S.-W. Kim, Transparent flexible stretchable piezoelectric and triboelectric nanogenerators for powering portable electronics, Nano Energy. 14 (2015) 139–160. https://doi.org/10.1016/j.nanoen.2014.11.009.
[42] Y. Hwan Ko, S. Hyun Lee, J. Woo Leem, J. Su Yu, High transparency and triboelectric charge generation properties of nano-patterned PDMS, RSC Advances. 4 (2014) 10216–10220. https://doi.org/10.1039/C3RA47199C.
[43] B.N. Chandrashekar, B. Deng, A.S. Smitha, Y. Chen, C. Tan, H. Zhang, H. Peng, Z. Liu, Roll-to-Roll Green Transfer of CVD Graphene onto Plastic for a Transparent and Flexible Triboelectric Nanogenerator, Advanced Materials. 27 (2015) 5210–5216. https://doi.org/10.1002/adma.201502560.
[44] H. Guo, Q. Leng, X. He, M. Wang, J. Chen, C. Hu, Y. Xi, A Triboelectric Generator Based on Checker-Like Interdigital Electrodes with a Sandwiched PET Thin Film for Harvesting Sliding Energy in All Directions, Advanced Energy Materials. 5 (2015) 1400790. https://doi.org/10.1002/aenm.201400790.
[45] N. Kaur, J. Bahadur, V. Panwar, P. Singh, K. Rathi, K. Pal, Effective energy harvesting from a single electrode based triboelectric nanogenerator, Scientific Reports. 6 (2016) 38835. https://doi.org/10.1038/srep38835.
[46] Z.L. Wang, L. Lin, J. Chen, S. Niu, Y. Zi, Triboelectric Nanogenerator: Single-Electrode Mode, in: Z.L. Wang, L. Lin, J. Chen, S. Niu, Y. Zi (Eds.), Triboelectric Nanogenerators, Springer International Publishing, Cham, 2016: pp. 91–107. https://doi.org/10.1007/978-3-319-40039-6_4.
[47] S.W. Chen, X. Cao, N. Wang, L. Ma, H.R. Zhu, M. Willander, Y. Jie, Z.L. Wang, An Ultrathin Flexible Single-Electrode Triboelectric-Nanogenerator for Mechanical Energy Harvesting and Instantaneous Force Sensing, Advanced Energy Materials. 7 (2017) 1601255. https://doi.org/10.1002/aenm.201601255.
[48] K. Parida, V. Kumar, W. Jiangxin, V. Bhavanasi, R. Bendi, P.S. Lee, Highly Transparent, Stretchable, and Self-Healing Ionic-Skin Triboelectric Nanogenerators for Energy Harvesting and Touch Applications, Advanced Materials. 29 (2017) 1702181. https://doi.org/10.1002/adma.201702181.
[49] X. Wang, Y. Yin, F. Yi, K. Dai, S. Niu, Y. Han, Y. Zhang, Z. You, Bioinspired stretchable triboelectric nanogenerator as energy-harvesting skin for self-powered electronics, Nano Energy. 39 (2017) 429–436. https://doi.org/10.1016/j.nanoen.2017.07.022.
[50] Y. Yang, H. Zhang, Z.-H. Lin, Y.S. Zhou, Q. Jing, Y. Su, J. Yang, J. Chen, C. Hu, Z.L. Wang, Human Skin Based Triboelectric Nanogenerators for Harvesting Biomechanical Energy and as Self-Powered Active Tactile Sensor System, ACS Nano. 7 (2013) 9213–9222. https://doi.org/10.1021/nn403838y.
[51] T. Huang, C. Wang, H. Yu, H. Wang, Q. Zhang, M. Zhu, Human walking-driven wearable all-fiber triboelectric nanogenerator containing electrospun polyvinylidene fluoride piezoelectric nanofibers, Nano Energy. 14 (2015) 226–235. https://doi.org/10.1016/j.nanoen.2015.01.038.
[52] W. Yang, J. Chen, G. Zhu, J. Yang, P. Bai, Y. Su, Q. Jing, X. Cao, Z.L. Wang, Harvesting Energy from the Natural Vibration of Human Walking, ACS Nano. 7 (2013) 11317–11324. https://doi.org/10.1021/nn405175z.
[53] Y. Zi, J. Wang, S. Wang, S. Li, Z. Wen, H. Guo, Z.L. Wang, Effective energy storage from a triboelectric nanogenerator, Nature Communications. 7 (2016) 10987. https://doi.org/10.1038/ncomms10987.
[54] The Triboelectric Series - AlphaLab, Inc, AlphaLab, Inc. (n.d.). https://www.alphalabinc.com/triboelectric-series/ (accessed February 25, 2019).
[55] S. Rathore, S. Sharma, B.P. Swain, R.K. Ghadai, A Critical Review on Triboelectric Nanogenerator, IOP Conf. Ser.: Mater. Sci. Eng. 377 (2018) 012186. https://doi.org/10.1088/1757-899X/377/1/012186.

[56] A.F. Diaz, R.M. Felix-Navarro, A semi-quantitative tribo-electric series for polymeric materials: the influence of chemical structure and properties, Journal of Electrostatics. 62 (2004) 277–290. https://doi.org/10.1016/j.elstat.2004.05.005.
[57] H. Zou, Y. Zhang, L. Guo, P. Wang, X. He, G. Dai, H. Zheng, C. Chen, A.C. Wang, C. Xu, Z.L. Wang, Quantifying the triboelectric series, Nature Communications. 10 (2019) 1–9. https://doi.org/10.1038/s41467-019-09461-x.
[58] H.-J. Yoon, H. Ryu, S.-W. Kim, Sustainable powering triboelectric nanogenerators: Approaches and the path towards efficient use, Nano Energy. 51 (2018) 270–285. https://doi.org/10.1016/j.nanoen.2018.06.075.
[59] W. Du, X. Han, L. Lin, M. Chen, X. Li, C. Pan, Z.L. Wang, A Three Dimensional Multi-Layered Sliding Triboelectric Nanogenerator, Advanced Energy Materials. 4 (2014) 1301592. https://doi.org/10.1002/aenm.201301592.
[60] X. Pu, M. Liu, X. Chen, J. Sun, C. Du, Y. Zhang, J. Zhai, W. Hu, Z.L. Wang, Ultrastretchable, transparent triboelectric nanogenerator as electronic skin for biomechanical energy harvesting and tactile sensing, Science Advances. 3 (2017) e1700015. https://doi.org/10.1126/sciadv.1700015.
[61] Dscout Research: people touch cellphones 2,617 times a day - Business Insider, (n.d.). https://www.businessinsider.com/dscout-research-people-touch-cell-phones-2617-times-a-day-2016-7 (accessed July 18, 2019).
[62] C.B. Crawford, B. Quinn, 4 - Physiochemical properties and degradation, in: C.B. Crawford, B. Quinn (Eds.), Microplastic Pollutants, Elsevier, 2017: pp. 57–100. https://doi.org/10.1016/B978-0-12-809406-8.00004-9.
[63] M. Leonhard, J. Lin, S. Huang, Touch screen protector, US8044942B1, 2011. https://patents.google.com/patent/US8044942B1/en (accessed July 21, 2019).
[64] J.Y. Lee, Y.S. Oh, H.J. PARK, S.H. Kim, Large-size touch screen, US20110216020A1, 2011. https://patents.google.com/patent/US20110216020A1/en (accessed July 21, 2019).
[65] H.-C. Hsieh, J.-Y. Chen, W.-Y. Lee, D. Bera, W.-C. Chen, Stretchable Fluorescent Polyfluorene/Acrylonitrile Butadiene Rubber Blend Electrospun Fibers through Physical Interaction and Geometrical Confinement, Macromolecular Rapid Communications. 39 (2018) 1700616. https://doi.org/10.1002/marc.201700616.
[66] T. Yasin, S. Ahmed, M. Ahmed, F. Yoshii, Effect of concentration of polyfunctional monomers on physical properties of acrylonitrile–butadiene rubber under electron-beam irradiation, Radiation Physics and Chemistry. 73 (2005) 155–158. https://doi.org/10.1016/j.radphyschem.2004.07.009.
[67] J.-M. Andanson, S.G. Kazarian, In situ ATR-FTIR Spectroscopy of Poly(ethylene terephthalate) Subjected to High-Temperature Methanol, Macromol. Symp. 265 (2008) 195–204. https://doi.org/10.1002/masy.200850521.
[68] M. Mecozzi, L. Nisini, The differentiation of biodegradable and non-biodegradable polyethylene terephthalate (PET) samples by FTIR spectroscopy: A potential support for the structural differentiation of PET in environmental analysis, Infrared Physics & Technology. 101 (2019) 119–126. https://doi.org/10.1016/j.infrared.2019.06.008.
[69] K. Elnagar, T. Abou Elmaaty, S. Raouf, Dyeing of Polyester and Polyamide Synthetic Fabrics with Natural Dyes Using Ecofriendly Technique, Journal of Textiles. (2014). https://doi.org/10.1155/2014/363079.
[70] A. a. M. El-Saftawy, Regulating The Performance Parameters Of Accelerated Particles, (2013). http://inis.iaea.org/Search/search.aspx?orig_q=RN:46135147 (accessed July 25, 2019).
[71] S. Samantarai, A. Nag, N. Singh, D. Dash, A. Basak, G.B. Nando, N.C. Das, Chemical modification of nitrile rubber in the latex stage by functionalizing phosphorylated cardanol prepolymer: A bio-based plasticizer and a renewable resource, Journal of Elastomers & Plastics. 51 (2019) 99–129. https://doi.org/10.1177/0095244318768644.

[72] A. Alhareb, H. Akil, Z. Ahmad, Poly(methyl methacrylate) denture base composites enhancement by various combinations of nitrile butadiene rubber/treated ceramic fillers, Journal of Thermoplastic Composite Materials. 30 (2017) 1069–1090. https://doi.org/10.1177/0892705715616856.
[73] Y. Zou, P. Tan, B. Shi, H. Ouyang, D. Jiang, Z. Liu, H. Li, M. Yu, C. Wang, X. Qu, L. Zhao, Y. Fan, Z.L. Wang, Z. Li, A bionic stretchable nanogenerator for underwater sensing and energy harvesting, Nature Communications. 10 (2019) 2695. https://doi.org/10.1038/s41467-019-10433-4.
[74] L. Gu, N. Cui, L. Cheng, Q. Xu, S. Bai, M. Yuan, W. Wu, J. Liu, Y. Zhao, F. Ma, Y. Qin, Z.L. Wang, Flexible Fiber Nanogenerator with 209 V Output Voltage Directly Powers a Light-Emitting Diode, Nano Lett. 13 (2013) 91–94. https://doi.org/10.1021/nl303539c.
[75] X. Wang, B. Yang, J. Liu, Y. Zhu, C. Yang, Q. He, A flexible triboelectric-piezoelectric hybrid nanogenerator based on P(VDF-TrFE) nanofibers and PDMS/MWCNT for wearable devices, Scientific Reports. 6 (2016) 36409. https://doi.org/10.1038/srep36409.
[76] M. Murai, H.-K. Lau, B.P. Pereira, R.W.H. Pho, A cadaver study on volume and surface area of the fingertip, The Journal of Hand Surgery. 22 (1997) 935–941. https://doi.org/10.1016/S0363-5023(97)80094-9.
[77] K. Parida, G. Thangavel, G. Cai, X. Zhou, S. Park, J. Xiong, P.S. Lee, Extremely stretchable and self-healing conductor based on thermoplastic elastomer for all-three-dimensional printed triboelectric nanogenerator, Nature Communications. 10 (2019) 2158. https://doi.org/10.1038/s41467-019-10061-y.
[78] C. Ramon, P. Garguilo, E.A. Fridgeirsson, J. Haueisen, Changes in scalp potentials and spatial smoothing effects of inclusion of dura layer in human head models for EEG simulations, Front Neuroeng. 7 (2014). https://doi.org/10.3389/fneng.2014.00032.
[79] A. Boonbumrung, P. Sae-oui, C. Sirisinha, Reinforcement of Multiwalled Carbon Nanotube in Nitrile Rubber: In Comparison with Carbon Black, Conductive Carbon Black, and Precipitated Silica, Journal of Nanomaterials. (2016). https://doi.org/10.1155/2016/6391572.
[80] Y. Zhu, B. Yang, J. Liu, X. Wang, L. Wang, X. Chen, C. Yang, A flexible and biocompatible triboelectric nanogenerator with tunable internal resistance for powering wearable devices, Scientific Reports. 6 (2016) 22233. https://doi.org/10.1038/srep22233.
[81] G. Hassan, F. Khan, A. Hassan, S. Ali, J. Bae, C.H. Lee, A flat-panel-shaped hybrid piezo/triboelectric nanogenerator for ambient energy harvesting, Nanotechnology. 28 (2017) 175402. https://doi.org/10.1088/1361-6528/aa65c3.
[82] H. Zhang, Y. Yang, T.-C. Hou, Y. Su, C. Hu, Z.L. Wang, Triboelectric nanogenerator built inside clothes for self-powered glucose biosensors, Nano Energy. 2 (2013) 1019–1024. https://doi.org/10.1016/j.nanoen.2013.03.024.
[83] D. Yoo, E.Y. Go, D. Choi, J.-W. Lee, I. Song, J.-Y. Sim, W. Hwang, D.S. Kim, Increased Interfacial Area between Dielectric Layer and Electrode of Triboelectric Nanogenerator toward Robustness and Boosted Energy Output, Nanomaterials. 9 (2019) 71. https://doi.org/10.3390/nano9010071.
[84] C. Cui, X. Wang, Z. Yi, B. Yang, X. Wang, X. Chen, J. Liu, C. Yang, Flexible Single-Electrode Triboelectric Nanogenerator and Body Moving Sensor Based on Porous Na2CO3/Polydimethylsiloxane Film, ACS Appl. Mater. Interfaces. 10 (2018) 3652–3659. https://doi.org/10.1021/acsami.7b17585.
[85] X. Hu, S. Li, H. Peng, A comparative study of equivalent circuit models for Li-ion batteries, Journal of Power Sources. 198 (2012) 359–367. https://doi.org/10.1016/j.jpowsour.2011.10.013.
[86] L. Lu, X. Han, J. Li, J. Hua, M. Ouyang, A review on the key issues for lithium-ion battery management in electric vehicles, Journal of Power Sources. 226 (2013) 272–288. https://doi.org/10.1016/j.jpowsour.2012.10.060.

[87] E.R. Delay, A.J. Golden, N.O. Steiner, A compact IC tone generator, Physiology & Behavior. 21 (1978) 133–134. https://doi.org/10.1016/0031-9384(78)90288-3.
[88] G. Zhu, Z.-H. Lin, Q. Jing, P. Bai, C. Pan, Y. Yang, Y. Zhou, Z.L. Wang, Toward Large-Scale Energy Harvesting by a Nanoparticle-Enhanced Triboelectric Nanogenerator, Nano Lett. 13 (2013) 847–853. https://doi.org/10.1021/nl4001053.
[89] M. Tsuji, S. Hikino, R. Tanabe, Y. Sano, Synthesis of Bicompartmental Ag/Cu Nanoparticles Using a Two-step Polyol Process, Chem. Lett. 38 (2009) 860–861. https://doi.org/10.1246/cl.2009.860.
[90] T. Shen, Y. Liu, Y. Zhu, D.-Q. Yang, E. Sacher, Improved adhesion of Ag NPs to the polyethylene terephthalate surface via atmospheric plasma treatment and surface functionalization, Applied Surface Science. 411 (2017) 411–418. https://doi.org/10.1016/j.apsusc.2017.03.149.
[91] J.A. Adekoya, E.O. Dare, M.A. Mesubi, Tunable morphological properties of silver enriched platinum allied nanoparticles and their catalysed reduction of p-nitrophenol, Adv. Nat. Sci: Nanosci. Nanotechnol. 5 (2014) 035007. https://doi.org/10.1088/2043-6262/5/3/035007.

Synthesis and Fabrication of Self-sustainable Triboelectric Energy Case for Powering Smart Electronic Devices

Highlights

- PET and NBR based single electrode Triboelectric Nanogenerators have been developed
- The nanogenerators were integrated to fabricate a self-sustainable energy case to power smart electronics through tapping and stepping motion
- The output of the energy case was tested for variable load frequency, airgap and finger combination
- The maximum output voltage was recorded to be 50.8 for the back part
- The device was further modified and tested using Ag nanoparticles

Declaration of interests

☒ The authors declare that they have no known competing financial interests or personal relationships that could have appeared to influence the work reported in this paper.

☐The authors declare the following financial interests/personal relationships which may be considered as potential competing interests: